This is a preprint version of the article published in:
Journal of the Acoustical Society of America, Vol. 137, No. 4, pp. 1790-1801 (2015).
http://dx.doi.org/10.1121/1.4915475

Please, cite this document as:
T. G. ZIELIŃSKI. "Generation of random microstructures and prediction of sound velocity and absorption for open foams with spherical pores." *Journal of the Acoustical Society of America*, Vol. **137**, No. 4, pp. 1790-1801 (2015).
DOI: 10.1121/1.4915475

Generation of random microstructures and prediction of sound velocity and absorption for open foams with spherical pores

TOMASZ G. ZIELIŃSKI
Institute of Fundamental Technological Research, Polish Academy of Sciences
ul. Pawinskiego 5B, 02-106 Warsaw, Poland
e-mail: tzielins@ippt.pan.pl

Abstract

This paper proposes and discusses an approach for the design and quality inspection of the morphology dedicated for sound absorbing foams, using a relatively simple technique for a random generation of periodic microstructures representative for open cell foams with spherical pores. The design is controlled by a few parameters, namely, the total open porosity and the average pore size, as well as the standard deviation of pore size. These design parameters are set up exactly and independently, however, the setting of the standard deviation of pore sizes requires some number of pores in the Representative Volume Element (RVE); this number is a procedure parameter. Another pore structure parameter which may be indirectly affected is the average size of windows linking the pores, however, it is in fact weakly controlled by the maximal pore-penetration factor, and moreover, it depends on the porosity and pore size. The proposed methodology for testing microstructure-designs of sound absorbing porous media applies the multi-scale modelling where some important transport parameters – responsible for sound propagation in a porous medium – are calculated from microstructure using the generated RVE, in order to estimate the sound velocity and absorption of such a designed material.

Key words: porous microstructure, sound absorption, open cell foams, multiscale modelling.

I. INTRODUCTION

Computational experiments can be an important tool for studying and designing novel materials with respect to some desirable macroscopic properties which essentially depend on the material's microstructure. This is especially true in the case of porous media which are typically characterized by a rather complex morphology involving some random factors. The stochastic generation of pore structures has been a subject of numerous research with respect to many problems like the Darcy flow [1], or the problems of elasticity and viscoelasticity of porous solids [2], or the effective electric conductivity of porous media [3], etc. However, the so-called transport parameters of porous media relevant for viscus and thermal flows are also responsible for an overall sound absorbing properties of porous materials with open porosity. The effects of microstructure for the transport parameters have been recently studied with respect to the reticulated foams, especially, polyurethane foams [4–8], but also some highly porous open-cell metallic foams [9]. Such reticulated foams are characterised by a very specific geometry of cells which can be idealized by tetrakaidecahedra shapes (Kelvin cells) or truncated octahedron networks with tetrahedral vertices. On the other hand, it has been reported that in case of some open-cell ceramic foams the shapes of pores tend to be spherical and the pores are linked by circular windows [10].

The main purpose of this work is to present a methodology for a morphological design of sound absorbing foams. The proposed approach consists of two stages: (1) the generation of representative microstructures with open-porosity, and (2) the multi-scale modelling of acoustics of such open porous media filled with air. The generation of porous microstructure will involve a random factor, however, it will be at the same time controlled by some average (or macroscopic) morphological parameters. Moreover, it is assumed that the pores are spherical, which is in agreement with the mentioned *non*-reticulated foams produced by thermo-chemical processes (with or without mixing) with pores created by growing air-bubbles, like, for example, in porous corrundum ceramics [10,11]. Therefore, the technique for the generation of representative microstructures will be essentially based on the algorithms of random packing of hard spheres. This subject has been investigated by many authors [12–18]. Two main group of techniques are based on the so-called Random Sequential Addition (RSA) process [19], or on the Lubachevsky–Stillinger compression algorithm [20]. The technique applied in this paper is similar to the Lubachevsky–Stillinger algorithm which was originally proposed for two-dimensional discs [20]. In this algorithm the particles start with random positions and velocities, and as they move about they grow uniformly in size, from points to jammed disks [20].

Apart from the purely morphological assumption of spherical pores, it is also assumed that the skeleton (or frame) of open-porosity foams is rigid with respect to the physical phenomena responsible for sound propagation. This is true in the case of ceramic foams (and usually *not* true in the case of soft polyurethane foams, especially in some lower frequency range). Thus, the carrier medium for sound waves is only the air inside the open pore structure. In such a case of rigid porous medium, the propagation and absorption of sound can be described by the so-called fluid-equivalent models, i.a., by the very efficient and widely accepted Johnson-Allard model [21] which involves a semi-phenomenological modelling of the viscous effects by Johnson *et al.* [22] (with some enhancements by Pride *et al.* [23]), as well as a modelling involving thermal effects [24–26]. The efficiency of this rather complex model results from the fact that it was actually derived by referring to an average porous microstructure [26,27]. Such an approach has recently allowed for advanced microstructure-based analyses in poro-acoustics: by using some approximative two-dimensional representations of porous materials [28–30] and also more realistic three-dimensional representative cells [4,9,31–33]. In this approach some relevant finite element analyses carried out on the fluid domains in the periodic representative cells serve to calculate from microstructure some transport parameters (like: permeability and its thermal analogue, or viscous and thermal characteristic lengths, etc.) used by the Johnson-Allard model. Thus, the influence of microstructure on some of those parameters may now be also thoroughly studied [8,34,35] (separately from the whole poro-acoustic model). The authors of microstructure-based analyses usually propose very simplified periodic cells to represent the studied porous media; in the case of materials with spherical pores the representative micro-geometries are based on some regular sphere-packings [32,33]. For example, Chevillotte *et al.* [33] used the body-centered cubic (BCC) arrangement as the most appropriate for the physics of such foams, because it tends to the Kelvin cell (tetrakaidecahedron) when pores are growing (as in the case of high porosity polyurethane or polymer foams). The regular sphere packings have also been used in the microstructure-based modelling of porous media made up of rigid spheres [31,36–38], for which – in the case when the spheres are identical – even some analytical estimations of the relevant transport parameters are possible [37,39].

The present work is organized as follows. First, the procedure for a controlled random generation of periodic microstructures representative for open cell foams with spherical pores is presented. The main idea and important features of the proposed technique are discussed and illustrated with an example of the controlled generation of microstructure for an open-cell foam with the designed porosity of 70% and the average diameter of pores equal to 330 µm. In the second part of paper, this periodic Representative Volume Element is used to evaluate sound propagation and absorption in foams of such micro-geometry made up of a stiff material. To this end, first, some necessary transport parameters are calculated from the microstructure and they are used by the multiscale modelling to determine the effective speed of sound in the designed rigid foam, as well as the acoustic wave number and celerity. Then, the surface acoustic impedance and absorption are calculated from the effective model for rigid foam layers of various thicknesses. Finally, some limitations of the proposed approach are discussed in the context of the results obtained for a real ceramic foam with spherical pores and open porosity of 88%.

II. CONTROLLED RANDOM GENERATION OF PERIODIC MICROSTRUCTURES REPRESENTATIVE FOR FOAMS WITH SPHERICAL PORES

A. Procedure and design parameters

In order to calculate the parameters for the Johnson-Allard poro-acoustical model [21,26] one needs a small periodic cubic cell with a piece of skeleton (solid frame) inside. Such a cell must be representative for the (macroscopically homogeneous) porous medium to constitute its Representative Volume Element (RVE). Porous materials are usually not regular on the micro-scale level though their micro-geometry can be rather well described by some global

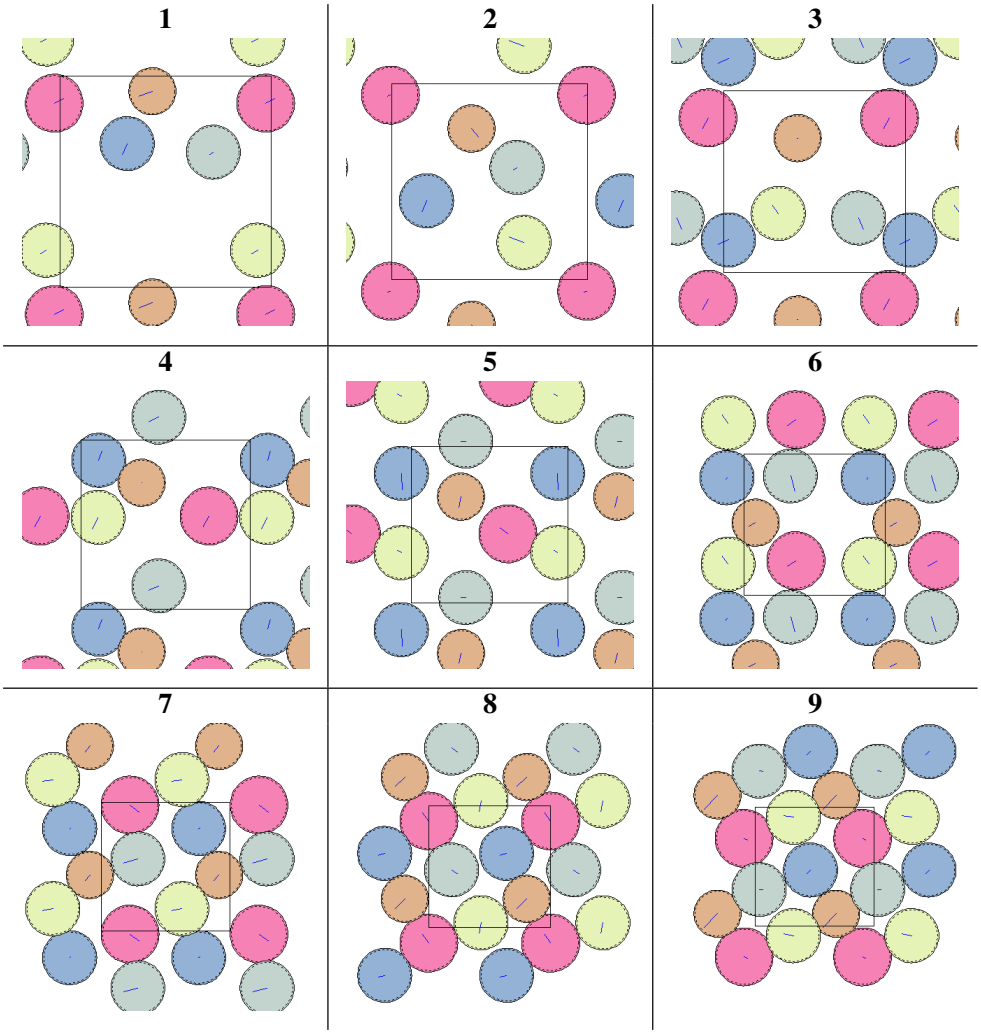

Figure 1: Periodic arrangements of moving bubbles

parameters like porosity, some generic features like typical shape of pores or fibres, and some statistical data like, for example, typical sizes of pores and windows linking the pores in case of foams, or typical size of fibres and distances between them in case of fibrous materials. Therefore, it seems reasonable that RVEs may be constructed in a random way basing on some typical statistics of real porous media they tend to represent.

A comparatively simple method of random generation of RVEs for foams with spherical pores is proposed here. First of all, the method relies on the dynamics of spherical bubbles (or in fact, rigid spheres) which move and bounce each other while the cubic cell of RVE decrease its size, and the whole procedure imposes the periodic boundary conditions. As mentioned above, this approach is similar to the Lubachevsky–Stillinger method[20] which is essentially a hard-sphere molecular dynamics with the particles growing in size during the course of the simulation at a certain expansion rate and colliding with each other elastically[14]. In the procedure proposed here, the bubbles (spheres) may freely pass the walls of the shrinking cube yet the whole setup is periodic so they at once appear from the other side. As a matter of fact each bubble/sphere belongs to an ensemble of eight identical bubbles set in the corners of a cube with its edge equal to the current edge-length of the RVE cell. (The edge of the cube changes together with the change of size of RVE.) These imposes some additional constraints, however, it is necessary to insure the periodicity of RVE. The (final) diameters of bubbles should be chosen to be consistent with the statistics of the real foam. There is also a penetration parameter which states how much the bubbles may penetrate each other; this parameter together with the assumed bubble sizes should yield typical sizes of windows linking the pores which are known form the foam statistics. Figure 1 depicts the idea in 2D, showing some periodic arrangements of moving bubbles in a few frames of motion (the solid square shows the boundary of periodic cell and the dashed circles inside the bubbles mark the maximal range of penetration). The whole procedure can be stopped when the global porosity is reached or when the size of the RVE cube cannot be decreased. It was found that to improve mixing and packing of spheres (bubbles, pores) specific techniques may involve: gravity simulation, bubble shrinking and swelling, random acceleration, collision energy dissipation, etc.

The proposed method ensures realistic random arrangements of pores because of some inherent aleatory factors and techniques mentioned above. Thus, also the initial distribution of spheres is random as well as their initial velocities. On the other hand, some macroscopic parameters of the porous microstructure need to be controlled. As such parameters are chosen: the total open porosity and the average size of pores. These two primary parameters are complemented by two auxiliary ones, namely: the standard devia-

tion of pore size and the penetration factor. The choice of primary parameters is rather obvious since the porosity and pore size are crucial for sound absorption and propagation in porous media, as well as for the chemical precesses of their production. In fact, those parameters are often controlled or designed factors in the manufacturing of real foams. It is important to notice here that those two parameters (in contrast to the auxiliary ones) will be controlled directly, precisely and independently.

Yet another feature of porous foams, namely, the typical size of windows linking the pores, will be indirectly controlled in the proposed procedure by means of the mentioned penetration factor. This dimensionless parameter ζ is defined here as the ratio of the maximal allowed penetration of a bubble (sphere) by neighbouring bubbles, to the actual radius of this bubble (see Figure 2). Its value limits in some way the final sizes of the widows linking pores.

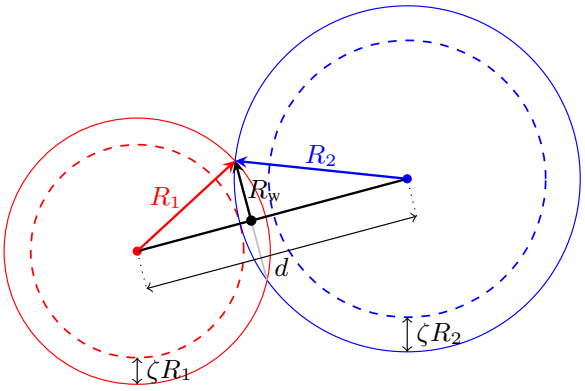

Figure 2: Two mutually penetrating spheres

Figure 2 shows two neighbouring spheres (pores): one with radius R_1 and the other with radius R_2. The distance d between them is smaller than the sum of their radii, i.e., $d < R_1 + R_2$, therefore, there is a circular window linking these pores and its radius is:

$$R_w = \frac{1}{2d}\sqrt{2d^2(R_1^2 + R_2^2) - (R_1^2 - R_2^2)^2 - d^4}\,. \qquad (1)$$

In the case when the spheres (pores) are of the same size, i.e., $R_1 = R_2 \equiv R_p$, the size of window with respect to the size of pores equals

$$\frac{R_w}{R_p} = \sqrt{1 - \frac{d^2}{4R_p^2}}\,. \qquad (2)$$

When the maximal allowed sphere-penetration ζR_p is reached, which means that the distance between two identical spheres is $d = R_p(2 - \zeta)$, the ratio of the widow size to the pore size equals

$$\frac{R_w}{R_p} = \sqrt{\zeta - \frac{\zeta^2}{4}} \qquad (3)$$

and it is a function of the dimensionless penetration factor ζ. Figure 3 plots this window-to-pore size ratio with respect to the value of penetration factor, in the full range from $\zeta = 0$ (when the spheres are in contact) to $\zeta = 2$ (when the spheres fully overlap), although practical values of ζ should be smaller than 1. The plot in Figure 3 permits to estimate that, for example, for $\zeta = 0.2$ the maximal window size should rather be smaller than 0.44 of the average size of pores, although this would depend also on the variation of pore sizes as well as on the total porosity and random

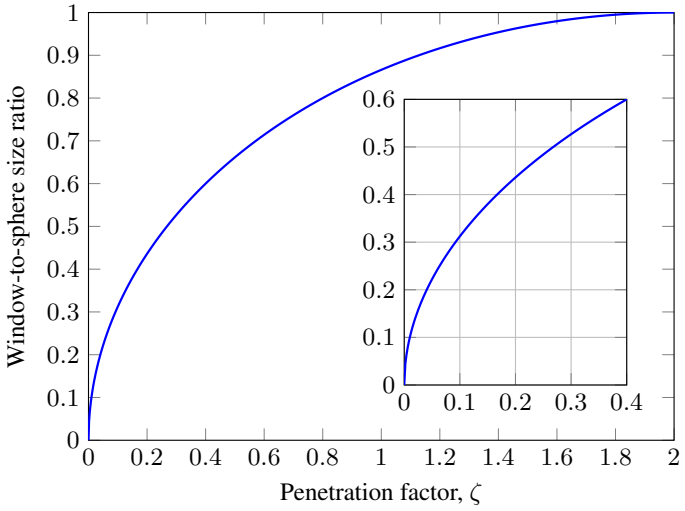

Figure 3: The ratio of window to sphere size with respect to the penetration factor (the case of two identical spheres)

mixing/packing. Nevertheless, this estimate is quite useful; however, when choosing the penetration factor ζ one should remember that the average window size would certainly be even smaller than the estimated limiting value.

It must be remarked here that the size of widows is also somehow dependent on the porosity and the typical pore size specified by the average pore-size with the standard deviation. In the proposed methodology the standard deviation of pore size can be approximately adjusted provided that there are at least a few different representative spherical pores in RVE. The size of spheres (which would become pores) can be semi-randomly or manually set in that way so that the standard deviation equals the required (or designed) value. Another possibility is to set for all the spheres the same initial size, i.e., the diameter (or radius) equal to 1, and then get some standard deviation by random swelling and/or shrinking the spheres during the dynamic periodic mixing in the shrinking cube of RVE. This second approach, however, would require some control of the swelling/shrinking rate. Finally, it has been found that a very convenient approach is the one where the initial sizes of spheres are assumed accordingly to some (initial) standard deviation value which may be slightly modified by comparatively slow random swelling/shrinking during the numerical packing process.

B. Foam microstructure with open porosity of 70%

In the example presented in this paper five spheres were used to generate a Representative Volume Element with the exact designed porosity of only 70% – with enough of the skeleton to ensure a good bearing capacity – to suggests a multi-functionality of such sound absorbing material. The size of spheres (in fact, their diameters) had been initially chosen as: 0.8, 0.9, 1.0, 1.1, and 1.2., which gives the mean value of 1 with the standard deviation of 0.1581. The same maximal penetration factor $\zeta = 0.2$ was set for all the spheres. Then, the dynamic periodic mixing and packing of spheres – under the law of elastic collision – inside the shrinking cubic space was effectuated. The spheres were allowed to slowly shrink and (even more slowly) swell, however, the rate of sphere shrinking/swelling was slower than the shrinking rate of RVE cube. At each step the porosity was calculated and the whole procedure

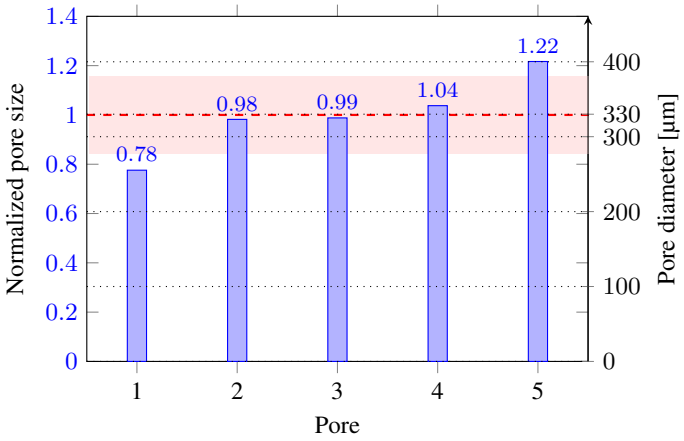

Figure 4: Pore sizes, their average diameter with the (band of) standard deviation

was terminated when its value reached 70%. The final size of spheres (pores) was normalized, so that their mean value was again exactly 1. These final normalized sizes of pores are shown in Figure 4. It appeared that the final standard deviation was 0.1574, that is, nearly the same as the initial one. Now, the average pore diameter was set to the exact designed value of 0.33 mm by simply rescaling the RVE cube: in order to achieve this its edge-length was set to 0.52 mm. The corresponding pore diameters are listed in Table I and they can also be read from Figure 4. Finally, Figure 5 presents typical size of windows linking the pores in the final RVE. (One should notice that there are 11 windows since some pores – each represented by an assembly of eight spheres during the dynamic mixing – could be linked by two different windows, because of periodicity.) By rescaling the RVE cube in order to set the designed pore size, the average diameter of windows was set to 0.136 mm with the standard deviation of 19% of this value. Thus, the ratio of the average window to average pore size equals 0.41.

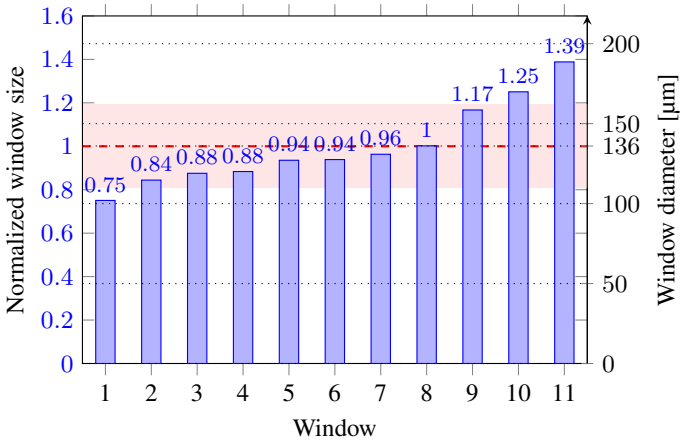

Figure 5: Window sizes, their average diameter with the (band of) standard deviation

Figure 6 shows the final random arrangement of pores (overlapping bubbles) in the periodic RVE with open porosity of 70%. Only those bubbles are shown which are in contact with the single RVE cube, and therefore, usually, less than eight bubbles from every assembly of each 'periodic pore'. The solid skeleton (frame) of such periodic representation of foam with porosity 70% is presented in

Table I: Geometric data of the randomly-generated periodic RVE for open-cell foam of porosity 70%

Porosity: **70%**	Number of pores in RVE: **5**		
Ratio of the pore diameters to the RVE edge-length: 0.4948 0.6263 0.6301 0.6618 0.7761			
Pore diameters [mm] for the RVE edge-length of **0.5159 mm**: 0.2553 0.3231 0.3251 0.3414 0.4004			
Average diameter [µm] of		windows: 136	pores: **330**
Volume [mm^3] of	RVE: 0.1373	frame: 0.0412	pores: 0.0961

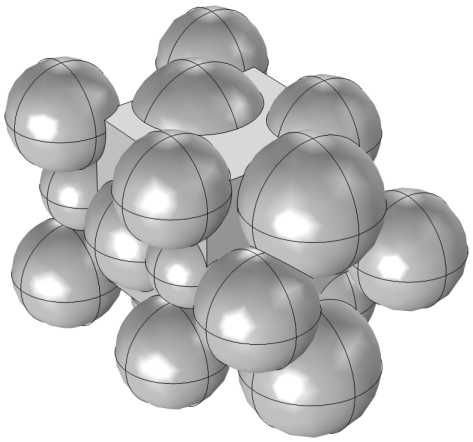

Figure 6: Randomly-generated periodic arrangement of bubbles (pores) in the cube of Representative Volume Element (RVE) for an open-cell foam with porosity 70%

Figure 7. In the top row there are three views at various angles of the original periodic cell with three tiny, seemingly disconnected fragments visible at lower part. In fact, they are not loose at all, but they are simply tiny parts from the relevant opposite sides of the periodic cubic cell. Such a representation with tiny bits of solid or fluid domains would be quite inconvenient for finite element meshing and analyses. Therefore, the original periodic cell was simply periodically shifted (by the vector $[0, 0.3, 0.3]$) to get a compact form of periodic skeleton visualised in the bottom row of Figure 7; the corresponding (shifted) RVE-cube has also been visualized in Figure 6. This shifted periodic cell was used in all finite element calculations. Some relevant geometric data of this periodic microstructure are listed in Table I.

III. SOUND PROPAGATION AND ABSORPTION IN RIGID FOAMS WITH OPEN POROSITY

A. Effective fluid

As mentioned above, the sound waves propagation in porous media with rigid frame can be very effectively modelled using the so-called fluid equivalent approach, where a porous material is substituted by an effective fluid. The dynamic density and dynamic bulk modulus of such fluid are frequency-dependent and complex quantities defined as follows[21,26]

$$\varrho_{\mathrm{e}}(\omega) = \frac{\varrho_{\mathrm{f}}\,\alpha(\omega)}{\phi}, \qquad K_{\mathrm{e}}(\omega) = \frac{K_{\mathrm{f}}}{\phi\,\beta(\omega)}, \tag{4}$$

that is, with respect to the real constant density ϱ_{f} and bulk modulus K_{f} of the actual fluid in pores (usually, the air). Here, $\omega = 2\pi f$ is the angular frequency (f is the frequency), and the dimensionless

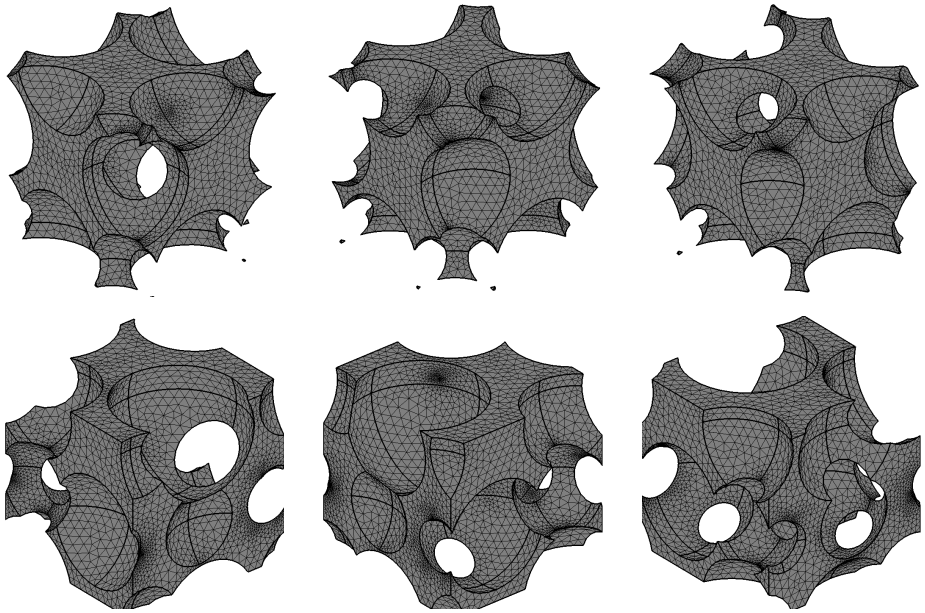

Figure 7: A randomly generated periodic cell of foam with open porosity 70% – three views of solid skeleton at various angles (top row), and these views of the same periodic cell shifted periodically by the vector $[0, 0.3, 0.3]$ (bottom row)

functions $\alpha(\omega)$ and $\beta(\omega)$ are the so-called dynamic tortuosity and the compressibility ratio (of the effective fluid to the pore-fluid), respectively. The dynamic tortuosity is the ratio of the dynamic density to the constant density of fluid in pores and is always greater than 1, since the effective fluid is virtually heavier than the actual pore-fluid because of some viscous and inertial interactions of fluid in pores with the solid frame. The compressibility ratio is derived as[21,26]

$$\beta(\omega) = \gamma_\mathrm{f} - \frac{\gamma_\mathrm{f} - 1}{\alpha'(\omega)}, \tag{5}$$

where γ_f is the specific heats ratio in pore-fluid, whereas $\alpha'(\omega)$ is the so-called dynamic *thermal* tortuosity of porous medium. This dimensionless function is a thermal analogue of the classic (i.e., *viscous*) dynamic tortuosity $\alpha(\omega)$.

The enhanced model by Johnson-Champoux-Allard-Pride-Lafarge provides the following formulas for the dynamic tortuosities[21,32]

$$\alpha(\omega) = \alpha_\infty + \frac{\nu_\mathrm{f}}{\mathrm{i}\omega}\frac{\phi}{k_0}\left[\sqrt{\frac{\mathrm{i}\omega}{\nu_\mathrm{f}}\left(\frac{2\alpha_\infty k_0}{\Lambda\phi}\right)^2 + b^2} - b + 1\right], \tag{6}$$

$$\alpha'(\omega) = 1 + \frac{\nu'_\mathrm{f}}{\mathrm{i}\omega}\frac{\phi}{k'_0}\left[\sqrt{\frac{\mathrm{i}\omega}{\nu'_\mathrm{f}}\left(\frac{2k'_0}{\Lambda'\phi}\right)^2 + b'^2} - b' + 1\right], \tag{7}$$

where

$$b = \frac{2\alpha_\infty^2 k_0}{\Lambda^2\phi(\alpha_0 - \alpha_\infty)}, \qquad b' = \frac{2k'_0}{\Lambda'^2\phi(\alpha'_0 - 1)}. \tag{8}$$

In the formulas above ν_f is the kinematic viscosity of pore-fluid and $\nu'_\mathrm{f} = \nu_\mathrm{f}/\mathrm{Pr}$ (Pr is the Prandtl number of fluid in pores), whereas all the other parameters are the so-called transport parameters of porous medium resulting purely from its micro-geometry. They are: the total porosity ϕ, the intrinsic (i.e., viscous) permeability k_0 and its thermal analogue k'_0, the intrinsic tortuosity α_∞ (i.e., purely inertial, in the high-frequency inviscid regime), the low-frequency limits of dynamic viscous tortuosity α_0 and dynamic thermal tortuosity α'_0, and finally, two characteristic lengths Λ and Λ' (for viscous forces and thermal effects, respectively).

B. Calculation of transport parameters from microstructure

The periodic arrangement of pores presented in Figure 6 together with the (conveniently shifted) cube yielded a good representative micro-geomertry for the designed open-cell foam with spherical pores. All pores are interconnected and they also form one single domain filled with the pore-fluid. Figure 8 shows the periodic skeleton as a unique non-fragmented solid domain, as well as a finite element mesh of the corresponding fluid domain. Such RVE served in all finite element analyses discussed below, necessary for determination of transport parameters used in the modelling of sound propagation in porous media.

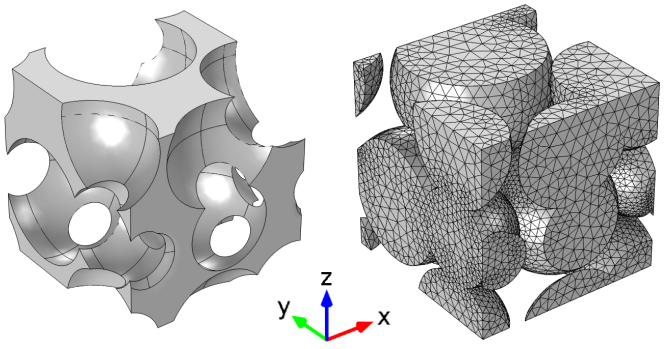

Figure 8: Randomly-generated periodic RVE for an open-cell foam with porosity 70%: the skeleton (frame) and a finite-element mesh of the corresponding fluid domain

The transport parameters are computed from three steady, static (i.e., non-harmonic) analyses defined on the fluid domain of Representative Volume Element; they are the following scaled Boundary Value Problems (BVPs)[4,26,31,37]:

- **the viscous flow problem:** the Stokes flow caused by a unit pressure gradient, with no-slip boundary conditions on the fluid-solid interface;
- **the thermal conduction problem:** a steady heat transfer caused by a unit heat source, with isothermal boundary conditions on the fluid-solid interface;
- **the electric conduction problem:** the electric field distribution in the fluid domain of porous medium made up of electrically insulating solid filled with a conductive fluid, caused by a unit electric potential gradient; in fact, the scaled electric conduction problem corresponds to the inertial flow in the high-frequency regime[4], and it can be eventually reduced to the Laplace problem for the unknown (electric) potential field.

The unit pressure gradient, unit heat source, and unit electric potential gradient are all *macroscopic* fields, i.e., constant throughout the fluid domain. The unknowns are relevant *microscopic* fields of velocity, temperature or electric potential, respectively, defined on the fluid domain, caused by the applied *macroscopic* fields.

The transport parameters are determined from the scaled solutions of those microstructural BVPs, averaged over the fluid domain, and using the appropriate formulas given for example in work by Zielinski[37]. Thus, the result of the viscous flow analysis shown in Figure 9 allowed to determine the parameter of static (viscous) permeability k_0 and the low-frequency limit α_0 (i.e., at 0 Hz) of the viscous dynamic tortuosity $\alpha(\omega)$. The result of the heat transfer analysis shown in Figure 10 permitted to calculate the thermal analogue of static permeability k_0' and the low-frequency limit α_0' of the thermal dynamic tortuosity $\alpha(\omega)$. Finally, from the result shown in Figure 11 – yielded by the Laplace analysis – the classical parameter of tortuosity α_∞ was calculated, which is, in fact, the high-frequency limit of the viscous dynamic tortuosity $\alpha(\omega)$, since the electric conduction problem of a porous medium formally coincides with the inviscid incompressible flow which captures the purely inertial resistance of flow through a porous medium at very high frequencies. From the solution of this problem also the viscous characteristic length Λ was determined. The thermal characteristic length Λ' is computed as the ratio of the doubled volume of fluid domain to the surface of fluid-solid inter-

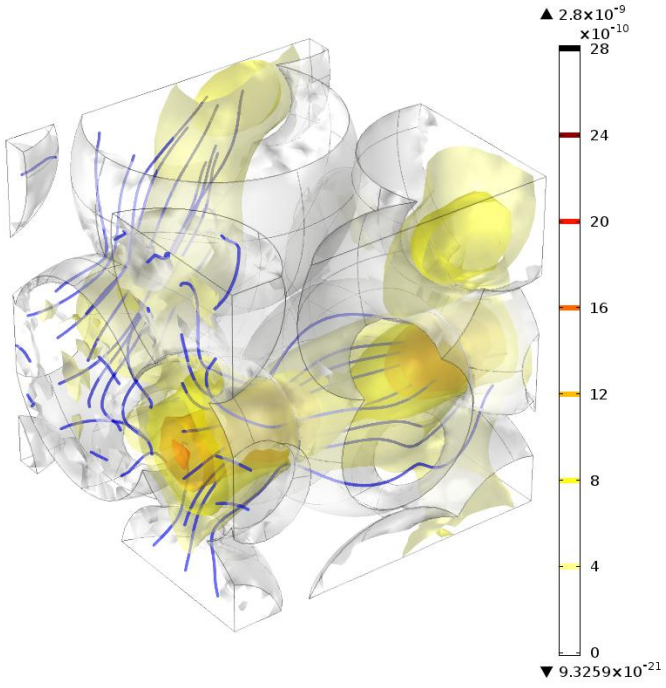

Figure 9: Viscous permeability field [m^2] (for the propagation direction X as shown in Figure 8) in the fluid domain of the randomly-generated RVE of foam with porosity 70%

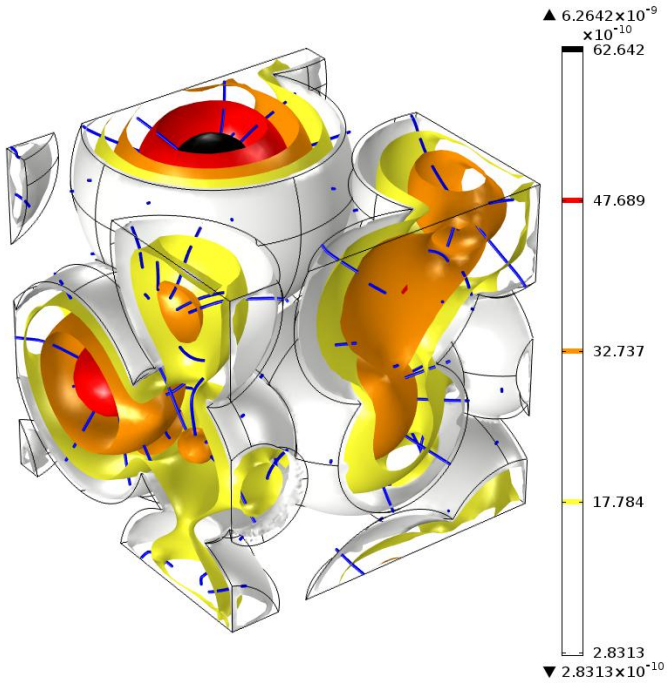

Figure 10: Thermal permeability field [m^2] for the randomly-generated RVE of foam with porosity 70%

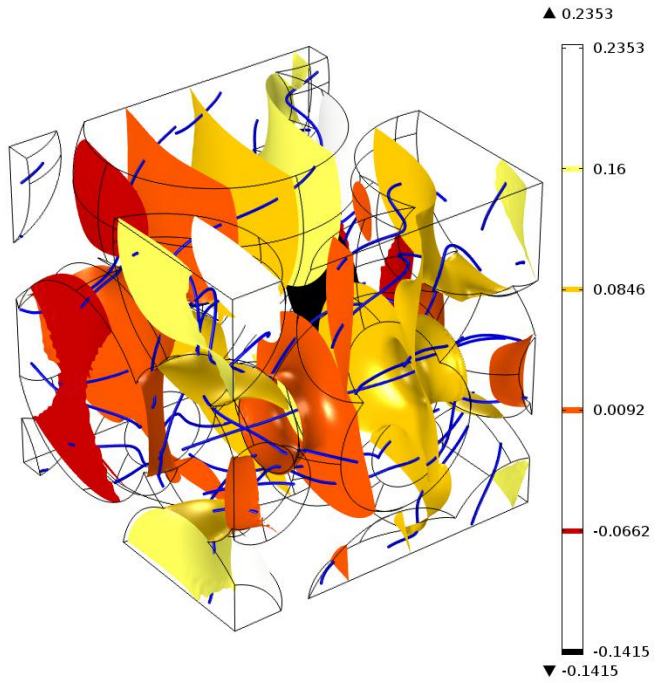

Figure 11: Potential field [m] (for the propagation direction X as shown in Figure 8) in the fluid domain of the randomly-generated RVE of foam with porosity 70%

face. All those necessary transport parameters determined from the randomly-generated representative microstructure of the designed foam are listed in Table II.

Table II: Transport parameters computed from microstructure for the randomly generated open foam with porosity 70%

Parameter	Symbol	Unit	Value
porosity	ϕ	%	69.980
tortuosity (at ∞ Hz)	α_∞	–	2.9518
viscous tortuosity at 0 Hz	α_0	–	3.9845
thermal tortuosity at 0 Hz	α'_0	–	1.4286
viscous permeability	k_0	10^{-10}m^2	2.0871
thermal permeability	k'_0	10^{-10}m^2	16.498
viscous characteristic length	Λ	10^{-6} m	70.335
thermal characteristic length	Λ'	10^{-6}m	138.32

C. Sound waves propagation in a rigid foam

The transport parameters computed from microstructure allowed to calculate the viscous and thermal dynamic tortuosities α and α', and then, the compressibility ratio β for the designed foam filled with air, using formulas given in Section A. Figure 12 presents the viscous dynamic tortuosity characteristics α in the wide frequency range from 10 Hz to 10 kHz; this dynamic tortuosity α describes in fact the density ratio of the effective equivalent fluid to the actual pore-fluid (air). Figure 13 presents the ratio of the bulk moduli of effective fluid and pore-fluid (air), which as a matter of fact, equals β^{-1}.

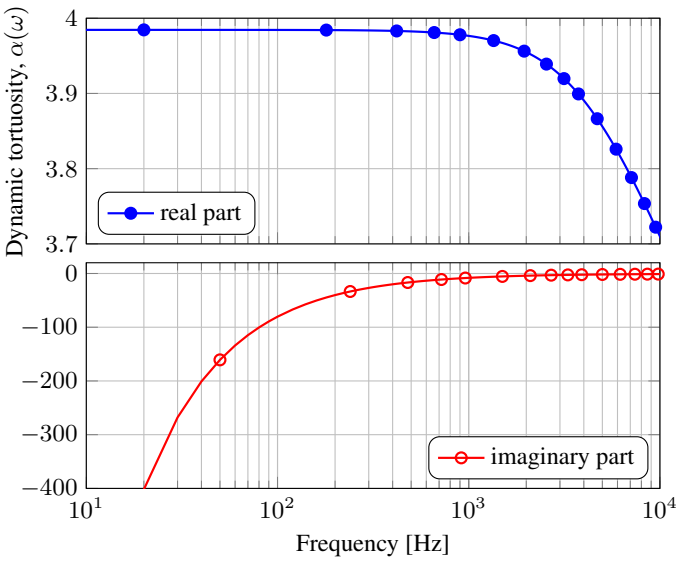

Figure 12: Dynamic viscous tortuosity (the ratio of the dynamic density to the density of pore-fluid, $\varrho_e(\omega)/\varrho_f = \alpha(\omega)$) for the foam with porosity 70%

The dynamic viscous tortuosity and compressibility ratio allow to determine the dynamic bulk modulus and density for the effective fluid equivalent to the designed foam filled with air, and then, the effective speed of sound in such a medium, which equals

$$c_e(\omega) = \sqrt{\frac{K_e(\omega)}{\varrho_e(\omega)}} = \frac{c_f}{\sqrt{\alpha(\omega)\beta(\omega)}}, \tag{9}$$

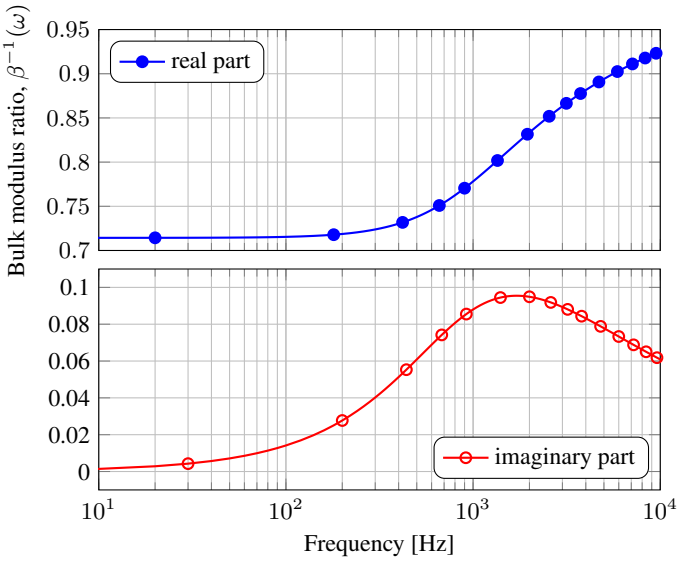

Figure 13: The ratio of the dynamic bulk modulus to the bulk modulus of pore-fluid, $K_e(\omega)/K_f = 1/\beta(\omega)$, for the foam with porosity 70%

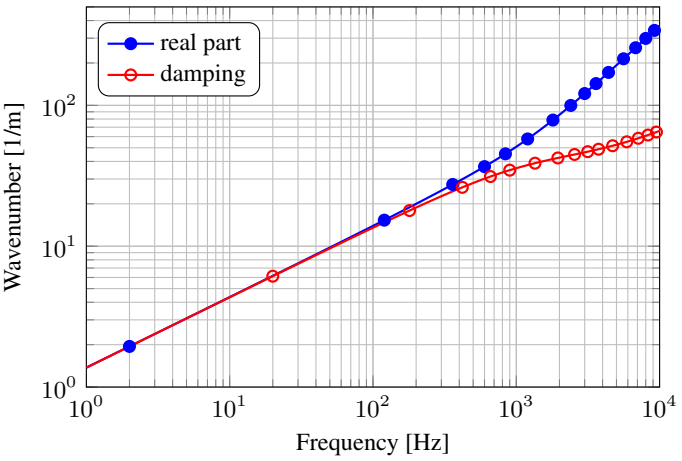

Figure 14: The complex wave number: its real part and the wave damping (equal to a minus imaginary part of the wave-number) for the foam with porosity 70%

where $c_f = \sqrt{K_f/\varrho_f} = \sqrt{\gamma_f P_f/\varrho_f}$ is the speed of sound in fluid in pores (air), and here, P_f is the ambient mean pressure. The effective speed of sound is a complex-valued function of frequency, and so is the corresponding effective wavenumber defined as

$$k_w = \frac{\omega}{c_e(\omega)} = \frac{\omega}{c_f}\sqrt{\alpha(\omega)\beta(\omega)}. \tag{10}$$

Figure 14 presents the complex wavenumber computed for the designed foam in the frequency range up to 10 kHz. The imaginary part of wavenumber is always negative, and therefore, in the logarithmic graph in Figure 14 the minus imaginary part is shown, which, as a matter of fact, represents the wave damping, since the complex wavenumber can be also expressed as follows

$$k_w = \frac{\omega}{c_w} - \mathrm{i}\, d_w, \tag{11}$$

where c_w is the wave celerity and d_w is the mentioned wave damping. Both these quantities are strongly frequency-dependent and they are calculated here from the following formulas based on the

determined wavenumber

$$c_{\mathrm{w}} = \frac{\omega}{\mathrm{Re}\, k_{\mathrm{w}}(\omega)}\,, \qquad d_{\mathrm{w}} = -\,\mathrm{Im}\, k_{\mathrm{w}}(\omega)\,. \tag{12}$$

One should notice that – since the effective density, bulk modulus and wave-number are complex – the first formula is *not* the same as $\mathrm{Re}(\omega/k_{\mathrm{w}}) = \mathrm{Re}\,\sqrt{K_{\mathrm{e}}/\varrho_{\mathrm{e}}} = \mathrm{Re}\, c_{\mathrm{e}}$ which is the real part of the complex effective speed of sound in the virtual fluid equivalent to porous medium.

The frequency-dependent variation of wave celerity is shown in Figure 15 where it is clear that it exhibits an asymptotic behaviour at limiting cases of extremely low and very high frequencies. Thus, the wave celerity reaches 171 m/s at 10 kHz, which is almost exactly one half of the assumed speed of sound $c_{\mathrm{f}} = 343$ m/s in air (pore-fluid) which fills the pore space; for even higher frequencies this value is only slightly exceeded. It is important to mention that the corresponding wave-lengths: 17.1 mm at 10 kHz, and approximately 8 mm at the audible upper-limit of 22 kHz, are always significantly greater than the characteristic sizes of pores listed in Table I. (The wave-length is computed as c_{w}/f, and the way it varies with frequency f is presented in Figure 16.) In a wide range of higher frequencies just below 10 kHz the wave celerity slightly decreases (see Figure 15), however, in a middle frequency range it starts to drop: at 3 kHz it is 155 m/s, and then only 124 m/s at 1 kHz. In fact, under 1 or 2 kHz it dramatically slows down to reach

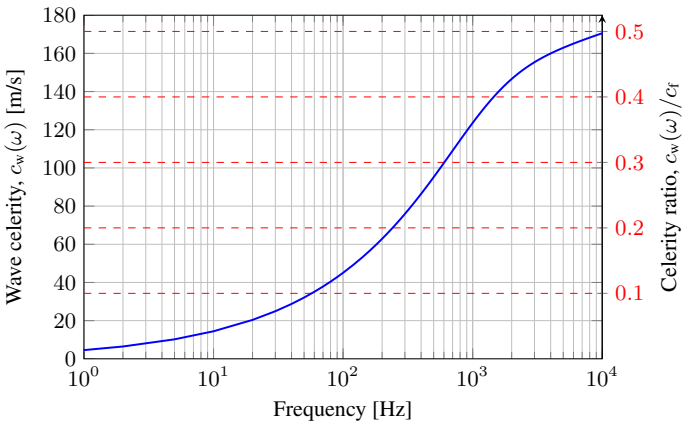

Figure 15: Acoustic wave celerity and its ratio with respect to the speed of sound in air (pore-fluid) for the foam with porosity 70%

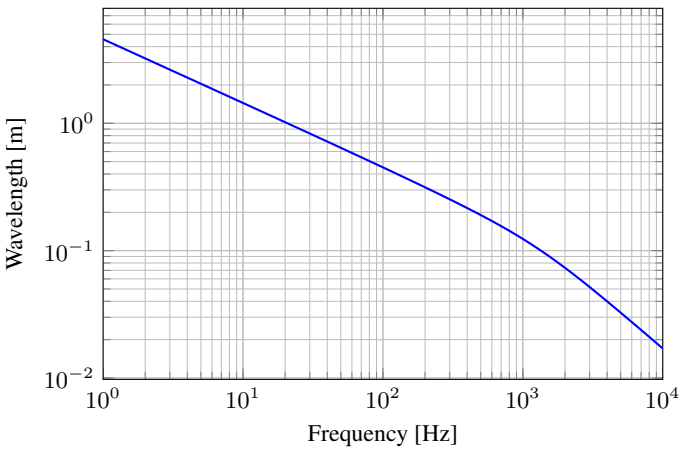

Figure 16: The variation of wave-length with frequency for the foam with porosity 70%

45 m/s at the frequency of 100 Hz. Then, the celerity curve asymptotically flattens and passes through 14 m/s at 10 Hz, to reach only 4.6 m/s at 1 Hz. This is very slow yet one should remember that the wave carrier medium is the pore-fluid only and a motionless "vacuum" of rigid skeleton fills 30% of the foam volume; moreover, the pores are rather very small, and although there are many of them, the microstructure is characterized by rather high tortuosity numbers (see Table II).

D. Surface acoustic impedance and absorption for rigid foam layers of various thickness

The homogenised microstructure-based model of porous material was used to estimate the sound absorption in the designed rigid foam of porosity 70%, by considering three layers of different thickness ℓ (set to a rigid wall), namely: $\ell = 20$ mm, 30 mm, and 40 mm. To this end, firstly, the surface acoustic impedance was calculated for each of three cases, using the following formula[21,40]

$$Z(\omega) = -\mathrm{i}\,\varrho_{\mathrm{e}}(\omega) c_{\mathrm{e}}(\omega)\,\cot\frac{\omega\ell}{c_{\mathrm{e}}(\omega)}. \tag{13}$$

The results presented for all three layers in Figure 17 show actually the ratio of the surface impedance $Z(\omega)$ to the characteristic impedance of air (pore-fluid) $Z_{\mathrm{f}} = 413.3$ Pa·s/m. The surface impedance for porous medium is complex, therefore for each case, two curves are shown: the real and imaginary parts of the impedance ratio.

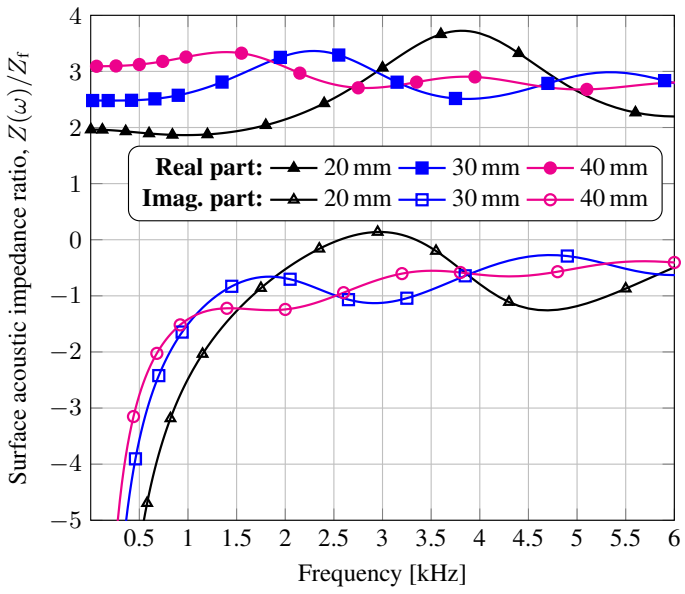

Figure 17: Surface acoustic impedance for the foam layers with open-cell porosity 70% and thickness of 20 mm, 30 mm and 40 mm

Basing on the results of surface acoustic impedance the acoustic absorption coefficient $A(\omega)$ was computed using the following formulas[21,40]

$$A(\omega) = 1 - |R(\omega)|^2, \quad \text{where} \quad R(\omega) = \frac{Z(\omega) - Z_{\mathrm{f}}}{Z(\omega) + Z_{\mathrm{f}}}. \tag{14}$$

Here, $R(\omega)$ is the frequency-dependent complex reflection coefficient which essentially depends on the surface impedance. The absorption coefficient $A(\omega)$ is a real-valued frequency-dependent quantity. Three absorption curves computed for three layers with

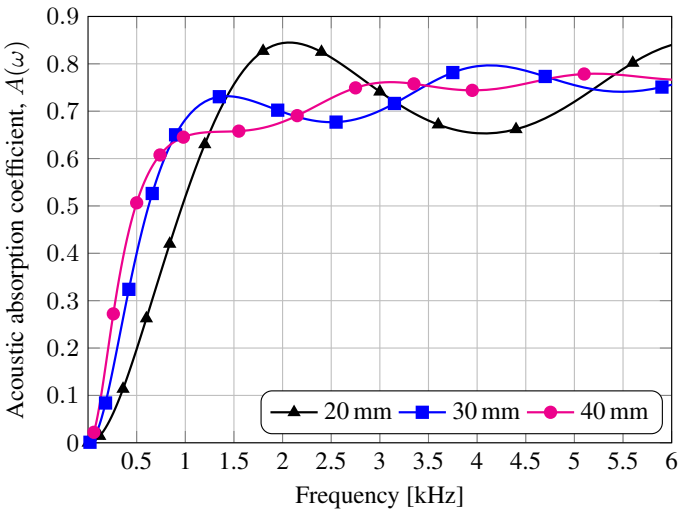

Figure 18: Acoustic absorption for the foam layers with open-cell porosity 70% and thickness of 20 mm, 30 mm and 40 mm

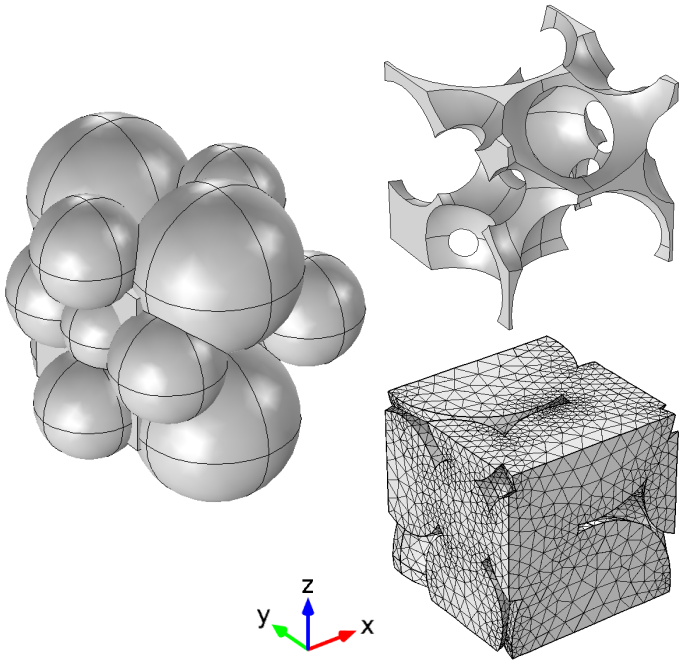

Figure 19: Periodic RVE for an open-cell foam with porosity 88%:, the periodic arrangement of bubbles (pores), the solid frame (skeleton) and a finite-element mesh of the corresponding fluid domain

the specified thickness – in the frequency range from 100 Hz to 6 kHz – are shown in Figure 18 to illustrate good sound absorption properties of the designed foam (cf. these results for example with the measurements of real foams in Zielinski *et al.*[11] or Zielinski and Rak[41]).

IV. LIMITATIONS

In this Section some limitations of the proposed approach will be discussed in the context of the results obtained for an existing ceramic foam.

A sample of alumina (aluminium oxide) ceramic foam of relatively high open porosity of 88% and the thickness of 16.5 mm was cut into a cylindrical shape with diameter of 29 mm, so that it could be fitted into the impedance tube, where the acoustic absorption coefficient for the sample was measured. As reported in Ref.[11] the size of minimum 150 pores and 350 windows was examined for such foam to assess that the pores are spherical in shape and their average diameter is 380 µm, whereas the average size of widows linking the pores is only 60 µm which gives a very small window-to-pore-size ratio of 0.16. Since, at the same time, the total porosity is relatively high, it means a rather large variety of pore sizes (i.e., there are very small pores/channels linking large pores and increasing the porosity).

In order to make the finite element calculations feasible the algorithm for random generation of representative microstructure was effectuated with only five pores of various sizes in a periodic cell and the standard deviation of pore size was 25% of the mean value. Thus, the microstructure with the required porosity of 88% could be generated only by assuming a higher penetration factor, so that the final window-to-pore-size ratio was 0.46. Figure 19 shows the final periodic arrangement of bubbles (pores) and the resulting periodic geometry of solid frame (skeleton) and fluid domain (with a visible mesh of finite elements).

Because of the restriction of the low number of complete pores (or, as a matter of fact, the reasonable number of degrees of freedom in finite element mesh), the generated microstructure seems to be only weakly representative for the ceramic foam. Therefore, two cases were investigated: (1) the Representative Volume Element RVE-1 set so that the average pore size is 380 µm, i.e., equal to the value reported for the ceramic foam, and in that case the average size of windows linking the pores is 176 µm; (2) the Representative Volume Element RVE-2 scaled so that the average pore size is 300 µm and the average size of windows linking the pores is 139 µm. For both cases, the transport parameters were calculated (for the propagation direction X) and they are presented in Table III. One may expect that the RVE-1 estimations may be rather correct (although slightly higher) in the case of thermal characteristic length and thermal permeability, while in the case of viscous characteristic length and permeability their values are certainly exaggerated, because the typical size of windows is much larger than in the ceramic foam. The scaling applied in the case of RVE-2 may to some extent alleviate that problem.

Table III: Transport parameters computed using two RVEs of different size and the same shape of microstructure with porosity 88%

Parameter	Symbol	Unit	RVE-1	RVE-2
porosity	ϕ	%	87.92	87.92
tortuosity (at ∞ Hz)	α_∞	–	1.264	1.266
viscous tortuosity at 0 Hz	α_0	–	1.892	1.898
thermal tortuosity at 0 Hz	α'_0	–	1.346	1.405
viscous permeability	k_0	10^{-9}m^2	1.199	0.746
thermal permeability	k'_0	10^{-9}m^2	3.999	2.845
viscous charact. length	Λ	10^{-6}m	125.2	97.60
thermal charact. length	Λ'	10^{-6}m	240.9	190.2

Figure 20 shows the acoustic absorption coefficient measured for the ceramic sample in the frequency range from 100 Hz to 6 kHz. The results are compared with the absorption curves determined numerically using the transport parameters calculated from RVE-1 or RVE-2. Although, as mentioned above, the periodic geometry is rather weakly representative for the ceramic foam, it ap-

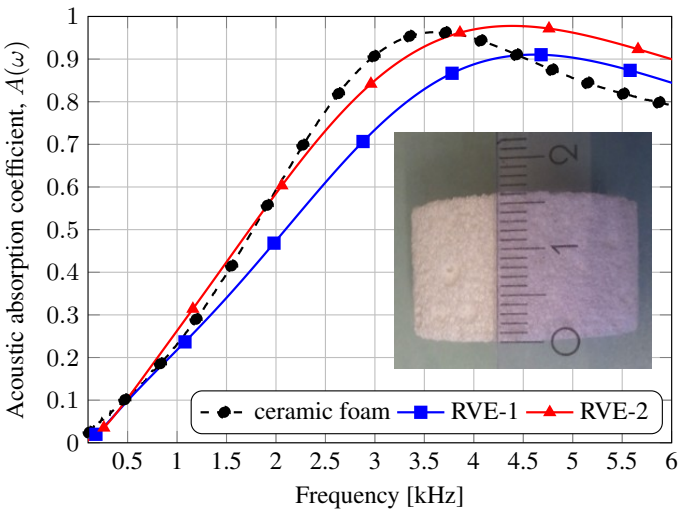

Figure 20: Acoustic absorption measured for a sample of ceramic foam with porosity 88% and thickness 16.5 mm, and the corresponding numerical results calculated for two Representative Volume Elements of the same geometrical shape but with different size (of pores)

pears that the numerical results are similar in character to the experimental curve, undoubtedly, because the most crucial parameters like the porosity, average size and shape of pores are exactly the same or very similar as in the real ceramic foam. (In case of the RVE-2 calculations, the discrepancies tend to be even acceptable.) Nevertheless, it is expected that a more representative micro-geometry should provide better results. In the case of the investigated ceramic foam such microstructure would certainly involve more pores (bubbles) with more diversified sizes (this may also require some additional techniques, for example, an initializing procedure which appropriately puts small bubbles between the large ones). Anyway, the main problem would be eventually the size of finite element mesh which may result in a very large number of degrees of freedom, especially, in the case of the viscous flow problem. Thus, one may conclude that the approach is now computationally suitable (especially) for foams with spherical pores of *not* very diversified sizes.

V. CONCLUSIONS

The methodology of rigorous estimation of sound velocity and absorption for foams with spherical pores, characterised by a few morphological parameters, has been discussed. It involves a semi-random generation of a representative microstructure described by the morphological parameters and then the microstructure-based multi-scale modelling of sound propagation in such a medium. The generation algorithm, which ensures the required periodicity of microstructure, is controlled by the designed open porosity and the penetration factor which describes the maximal allowed mutual penetration of neighbouring pores. The standard deviation of pore sizes is imposed directly by the initial sizes of spheres which eventually become pores. The main phase of the algorithm is finished when the designed value of porosity is achieved; then, the porous representative cell is re-scaled to set the desired value for the average pore size. In that way, the two main independent parameters: the total open porosity and the average pore size are exactly set. The dependent average value of windows linking the pores is approximately controlled by the penetration factor.

The multi-scale analysis of the generated exemplary microstructure of foam with the open porosity of 70% and average pore diameter 330 µm proved good sound absorbing properties of such a design, comparable to the sound absorption of rigid foams of much higher porosity of about 90%. On the other hand, the analysed design should certainly have better bearing capacity which may opt for a multi-functionality of such sound absorbing material.

It is proposed that new designs of sound absorbing foams should be tested in that way with at least a few randomly generated RVEs of the same typical features discussed above. Such approach should be more realistic with respect to the real foams than the one using manually generated (usually quite regular) RVEs. The proposed approach may be used for the optimization as well as sensitivity analyses in poro-acoustics with respect to some morphological parameters. Moreover, it is worth to note that the procedure for microstructure generation can also be used to construct periodic Representative Volume Elements for porous media composed from mixed rigid spheres of various size.

The discussed example of an existing ceramic foam with porosity 88% shows that a large number of pores (bubbles) with more diversified sizes may be required in order to generate representative microstructures for such foams. It means, however, a large RVE with very fine meshing and that would require more computational power. Moreover, the size of a large RVE may at higher frequencies become comparable with the wavelengths, which would worsen the accuracy and reliability of estimations, because of a weak separation of scales.

ACKNOWLEDGMENTS

This work was carried out in part using computing resources of the "*GRAFEN*" supercomputing cluster at the IPPT PAN, from the computer infrastructure of *Biocentrum Ochota*. Finite element calculations were effectuated using the *COMSOL Multiphysics* software at the IPPT PAN, funded in part from the Structural Funds in the Operational Programme – Innovative Economy (IE OP, Poland) financed from the European Regional Development Fund – the Project "Modern Material Technologies in Aerospace Industry", No. POIG.01.01.02-00-015/08. The author also wishes to thank Dr. Marek Potoczek from Rzeszów University of Technology for providing the ceramic material for the porous sample which served to produce the experimental curve presented in Figure 20.

[1] P. K. Smolarkiewicz and C. L. Winter, "Pores resolving simulation of Darcy flows," J. Comput. Phys. **229**, 3121–3133 (2010).

[2] M. I. El Ghezal, Y. Maalej, and I. Doghri, "Micromechanical models for porous and cellular materials in linear elasticity and viscoelasticity," Comput. Mater. Sci. **70**, 51–70 (2013).

[3] D. Roussel, A. Lichtner, D. Jauffrès, R. K. Bordia, and C. L. Martin, "Effective transport properties of 3D multi-component microstructures with interface resistance," Comp. Mater. Sci. **96**, 277–283 (2015).

[4] C. Perrot, F. Chevillotte, M. T. Hoang, G. Bonnet, F.-X. Bécot, L. Gautron, and A. Duval, "Microstructure, transport, and acoustic properties of open-cell foam samples. Experiments and three-dimensional numerical simulations," J. Appl. Phys. **111**, 014911 (2012).

[5] O. Doutres, N. Atalla, and K. Dong, "Effect of the microstructure closed pore content on the acoustic behavior of polyurethane foams," J. Appl. Phys. **110**, 064901 (2011).

[6] O. Doutres, N. Atalla, and K. Dong, "A semi-phenomenological model to

predict the acoustic behavior of fully and partially reticulated polyurethane foams," J. Appl. Phys. **113**, 054901 (2013).

[7] M. T. Hoang, G. Bonnet, H. T. Luu, and C. Perrot, "Linear elastic properties derivation from microstructures representative of transport parameters," J. Acoust. Soc. Am. **135**, 3172–3185 (2014).

[8] O. Doutres, M. Ouisse, N. Atalla, and M. Ichchou, "Impact of the irregular microgeometry of polyurethane foam on the macroscopic acoustic behavior predicted by a unit-cell model," J. Acoust. Soc. Am. **136**, 1666–1681 (2014).

[9] C. Perrot, R. Panneton, and X. Olny. "Periodic unit cell reconstruction of porous media: Application to open-cell aluminum foams," J. Appl. Phys. **101**, 113538 (2007).

[10] M. Potoczek, "Gelcasting of alumina foams using agarose solutions," Ceram. Int. **34**, 661–667 (2008).

[11] T. G. Zieliński, M. Potoczek, R. E. Śliwa, and Ł. J. Nowak, "Acoustic absorption of a new class of alumina foams with various high-porosity levels," Arch. Acoust. **38**, 495–502 (2013).

[12] J. G. Berryman, "Random close packing of hard spheres and disks," Phys. Rev. A: At., Mol., Opt. Phys. **27**, 1053–1061 (1983).

[13] S. Torquato and F. H. Stillinger, "Multiplicity of generation, selection, and classification procedures for jammed hard-particle packings," J. Phys. Chem. B, **105**, 11849–11853 (2001).

[14] A. Donev, S. Torquato, F. H. Stillinger, and R. Connelly, "Jamming in hard sphere and disk packings," J. Appl. Phys. **95**, 989–999 (2004).

[15] A. Donev, S. Torquato, F. H. Stillinger, and R. Connelly, "A linear programming algorithm to test for jamming in hard-sphere packings," J. Comput. Phys., **197**, 139–166 (2004).

[16] A. B. Hopkins, F. H. Stillinger, and S. Torquato, "Densest binary sphere packings," Phys. Rev. E: Stat., Nonlinear, Soft Matter Phys. **82**, 021130 (2012).

[17] V. Baranau and U. Tallarek, "Random-close packing limits for monodisperse and polydisperse hard spheres," Soft Matter **10**, 3826–3841 (2014).

[18] M. O'Keeffe, "Some properties of three-periodic sphere packings," Struct. Chem. **23**, 1079–1087 (2012).

[19] S. Torquato and F. H. Stillinger, "Exactly solvable disordered sphere-packing model in arbitrary-dimensional Euclidean spaces," Phys. Rev. E: Stat., Nonlinear, Soft Matter Phys. **73**, 031106 (2006).

[20] B. D. Lubachevsky and F. H. Stillinger, "Geometric properties of random disk packings," J. Stat. Phys. **60**, 561–583 (1990).

[21] J. F. Allard and N. Atalla, *Propagation of Sound in Porous Media: Modelling Sound Absorbing Materials, Second Edition* (John Wiley & Sons, UK, 2009), 372 pages.

[22] D. L. Johnson, J. Koplik, and R. Dashen, "Theory of dynamic permeability and tortuosity in fluid-saturated porous media," J. Fluid Mech. **176**, 379–402 (1987).

[23] S. R. Pride, F. D. Morgan, and A. F. Gangi, "Drag forces of porous-medium acoustics," Physical Review B **47**, 1964–4978 (1993).

[24] Y. Champoux and J.-F. Allard, "Dynamic tortuosity and bulk modulus in air-saturated porous media," J. Appl. Phys. **70**, 1975–1979 (1991).

[25] D. Lafarge, P. Lemarinier, J. F. Allard, and V. Tarnow, "Dynamic compressibility of air in porous structures at audible frequencies," J. Acoust. Soc. Am. **102**, 1995–2006 (1997).

[26] D. Lafarge, "The equivalent fluid model", in *Materials and Acoustics Handbook*, edited by M. Bruneau and C. Potel (ISTE, UK, John Wiley & Sons, USA, 2009), Chap. 6, pp. 167–201.

[27] D. Lafarge, *Propagation du son dans les matériaux poreux à structure rigide saturés par un fluide viscothermique* (*Sound Propagation in Porous Materials with Rigid Frame Saturated by a Visco-thermal Fluid*, in French) (Ph.D. dissertation, Université du Maine, France, 1993).

[28] C. Perrot, F. Chevillotte, and R. Panneton, "Bottom-up approach for microstructure optimization of sound absorbing materials," J. Acoust. Soc. Am. **124**, 940–948 (2008).

[29] C. Perrot, F. Chevillotte, and R. Panneton, "Dynamic viscous permeability of an open-cell aluminum foam: Computations versus experiments," J. Appl. Phys. **103**, 024909 (2008).

[30] F. Chevillotte, C. Perrot, and R. Panneton, "Microstructure based model for sound absorption predictions of perforated closed-cell metallic foams," J. Acoust. Soc. Am. **128**, 1766–1776 (2010).

[31] C.-Y. Lee, M. J. Leamy, and J. H. Nadler, "Acoustic absorption calculation in irreducible porous media: A unified computational approach," J. Acoust. Soc. Am. **126**, 1862–1870 (2009).

[32] T. G. Zieliński, "Inverse identification and microscopic estimation of parameters for models of sound absorption in porous ceramics," in *Proceedings of International Conference on Noise and Vibration Engineering (ISMA2012) / International Conference on Uncertainty in Structural Dynamics (USD2012)* edited by P. Sas, D. Moens, and S. Jonckheere (2012), pp. 95–108.

[33] F. Chevillotte, C. Perrot, and E. Guillon, "A direct link between microstructure and acoustical macro-behavior of real double porosity foams," J. Acoust. Soc. Am. **134**, 4681–4690 (2013).

[34] A. Cortis and J. G. Berryman, "Frequency-dependent viscous flow in channels with fractal rough surfaces," Phys. Fluids **22**, 053603 (2010).

[35] M. T. Hoang and C. Perrot, "Identifying local characteristic lengths governing sound wave properties in solid foams," J. Appl. Phys. **113**, 084905 (2013).

[36] S. Gasser, F. Paun, and Y. Bréchet, "Absorptive properties of rigid porous media: Application to face centered cubic sphere packing," J. Acoust. Soc. Am. **117**, 2090–2099 (2005).

[37] T. G. Zieliński, Microstructure-based calculations and experimental results for sound absorbing porous layers of randomly packed rigid spherical beads, J. Appl. Phys. **116**, 034905 (2014).

[38] H. Liasneuski, D. Hlushkou, S. Khirevich, A. Höltzel, U. Tallarek, and S. Torquato, "Impact of microstructure on the effective diffusivity in random packings of hard spheres," J. Appl. Phys. **116**, 034904 (2014).

[39] C. Boutin and C. Geindreau, "Periodic homogenization and consistent estimates of transport parameters through sphere and polyhedron packings in the whole porosity range," Phys. Rev. E: Stat., Nonlinear, Soft Matter Phys. **82**, 036313 (2010).

[40] T. G. Zieliński. "Numerical investigation of active porous composites with enhanced acoustic absorption," J. Sound Vib. **330**, 5292–5308 (2011).

[41] T. G. Zielinski and M. Rak. "Acoustic absorption of foams coated with MR fluid under the influence of magnetic field," J. Intell. Mater. Syst. Struct. **21**, 125–131 (2010).